A reduced-order-model-based equivalent circuit for piezoelectric micro-electro-mechanical-system loudspeakers modeling

C. Gazzola, V. Zega, A. Corigliano, Pierrick Lotton, M. Melon

FEBRUARY 20 2024

A reduced-order-model-based equivalent circuit for piezoelectric micro-electro-mechanical-system loudspeakers modeling

C. Gazzola ; V. Zega ; A. Corigliano ; P. Lotton; M. Melon

J. Acoust. Soc. Am. 155, 1503–1514 (2024)
https://doi.org/10.1121/10.0024939

JASA ARTICLE

A reduced-order-model-based equivalent circuit for piezoelectric micro-electro-mechanical-system loudspeakers modeling

C. Gazzola,[1] V. Zega,[1] A. Corigliano,[1,a)] P. Lotton,[2] and M. Melon[2]
[1]*Civil and Environmental Engineering Department, Politecnico di Milano, Milan, 20133, Italy*
[2]*Laboratoire d'Acoustique de l'Université du Mans (LAUM), UMR 6613, Institut d'Acoustique - Graduate School (IA-GS), CNRS, Le Mans Université, Le Mans, 72085, France*

ABSTRACT:
Piezoelectric micro-electro-mechanical-system (MEMS) speakers are emerging as promising implementations of loudspeakers at the microscale, as they are able to meet the ever-increasing requirements for modern audio devices to become smaller, lighter, and integrable into digital systems. In this work, we propose a finite element model (FEM)–assisted lumped-parameters equivalent circuit for a fast and accurate modeling of these types of devices. The electro-mechanical parameters are derived from a pre-stressed FEM eigenfrequency analysis, to account for arbitrarily complex geometries and for the shift of the speaker resonance frequency due to an initial non-null pre-deflected configuration. The parameters of the acoustical circuit are instead computed through analytical formulas. The acoustic short-circuit between the speaker front and rear sides is taken into account through a proper air-gaps modeling. The very good matching in terms of radiated sound pressure level among the equivalent circuit predictions, FEM simulations, and experimental data proves the ability of the proposed method to accurately simulate the speaker performance. Moreover, due to its generality, it represents a versatile tool for designing piezoelectric MEMS speakers. https://doi.org/10.1121/10.0024939
(Received 4 October 2023; revised 9 January 2024; accepted 31 January 2024; published online 20 February 2024)
[Editor: Laurent Maxit] Pages: 1503–1514

I. INTRODUCTION

Micro-electro-mechanical-system (MEMS) technology represents one of the major breakthroughs of the last century, fulfilling many important functions in mobile devices like smartphones, e.g., in the form of accelerometers, gyroscopes, and micro-mirrors. Acoustic MEMS have been the protagonists of an intense research work in recent years, due to the increased global demand for portable audio devices to become smaller and integrable into digital systems without impairing performance, such as sound quality or battery life. After the successful establishment of MEMS microphones as a state-of-the-art solution for mobile applications,[1] increasingly more attention is paid to the field of MEMS speakers.[2–4] Traditional microspeakers, like electrodynamic and balanced armature speakers, offer limited incremental improvements with respect to the ever-increasing requirements for modern devices to become smaller and lighter. On the other side, MEMS speakers, due to their intrinsic, small dimensions, integrability with on-chip circuits, and cost-efficiency in mass production, are emerging as very promising solutions.

Even if many MEMS loudspeaker configurations have been studied in the last years,[5–8] they are not yet competitive in terms of performance in free-field applications, with respect to their non-MEMS counterparts. Some piezoelectric MEMS speakers designed for in-ear applications have been instead capable to meet the market requirements.[9]

In 2018, Stoppel *et al.*[9] first proposed the mechanically-open and acoustically-closed (MOAC) design principle as a promising solution towards high-performance piezoelectric MEMS speakers. Since then, different structures with an arbitrarily complex path of air-gaps have been proposed.[10–12]

Lumped element modeling (LEM) and finite element analysis (FEA) can be used to predict the response of MEMS speakers. In the design phase, LEM models are preferable since three-dimensional (3D) fully coupled FEM simulations are extremely computationally demanding. The intrinsic multiphysics nature of the problem and the different mechanical layers constituting the MEMS device (for which thicknesses can differ of more than 1 order of magnitude), require indeed a high number of degrees of freedom and consequently, a prohibitive computational cost for the optimization stage.

LEM approaches rely instead on the representation of spatially distributed physical systems through a set of lumped elements, under the hypothesis that the length scale of the device is much smaller than the wavelength of the governing physical phenomenon. The acoustic wavelengths (17.1 m–17.1 mm for 20 Hz–20 kHz) for MEMS speakers are much greater than their sizes (1–10 mm) in almost the whole audible range. Moreover, the mechanical diaphragm

a)Email: alberto.corigliano@polimi.it

of MEMS loudspeakers is often designed to behave as a single-degree-of-freedom oscillator.[5,9,11,13–16] Single-degree-of-freedom lumped representations are hence sufficient to predict the response of these devices in almost the whole audible range.

Different contributions on equivalent circuital representations of microspeakers have been proposed[17–19] in the literature. Only very recently, these equivalent circuital representations based on an analytical estimation of the electro-mechano-acoustic lumped-parameters have been extended to piezoelectric MEMS speakers.[5,6,20] Wang *et al.*[6] proposed an equivalent circuit for different packaging configurations of a piezoelectric MEMS speaker based on thin ceramic lead zirconate titanate (PZT) composed of a clamped circular plate. Liechti *et al.*[5,20] proposed a lumped equivalent network for a two wafers pieozoelectric MEMS speaker, whose radiating element is composed of a rigid plate surrounded by a small interstice of air.

The mechanical diaphragm of different MEMS loudspeakers is however composed of fairly complex geometries[11,21] defined by the chosen air-gaps path, for which an analytical estimation of the electro-mechanical parameters is not straightforward and not practical for a design optimization procedure.

In this work, we propose a FEM-assisted lumped-parameters equivalent circuit to simulate the free-field and in-ear response of piezoelectric MEMS speakers. The novelty relies in the hybrid approach adopted to estimate the LEM parameters. The electro-mechanical parameters are extracted from a reduced order model (ROM), which is obtained by the projection of the equations of motion on the pre-stressed undamped electro-mechanical eigenmode of the loudspeaker computed via FEM, while acoustical parameters are derived through analytical formulas. The FEM-based estimation of the electro-mechanical parameters allows us to account for arbitrarily complex geometries and for the shift of the speaker resonance frequency due to an initial non-null pre-deflected configuration. In the acoustic domain, the acoustic short-circuit effect between the speaker front and rear sides is included through an analytical description of the air-gaps behaviour.

The equivalent circuit predictions are compared with full-order FEM simulations (for free-field and in-ear conditions) and with experimental results (for in-ear conditions), performed on the piezoelectric MEMS speaker recently proposed in Gazzola *et al.*[10]

The paper is organized as follows: the reference design exploited to validate the proposed equivalent circuit is presented in Sec. II. The lumped element model for free-field and in-ear conditions along with the derivation of the electro-mechanical and acoustical lumped-elements are detailed in Sec. III. LEM predictions are compared to full-FEM results in Sec. IV and to experimental results in Sec. V. Finally, in Sec. VI, conclusions are drawn together with future perspectives.

II. REFERENCE LOUDSPEAKER

The MEMS loudspeaker recently proposed in Gazzola *et al.*[10] is here employed to validate the modeling approach based on the proposed hybrid LEM. The moving mechanical structure consists of four trapezoidal actuators connected to a central squared piston through a set of properly sized folded elastic springs as schematically reported in Fig. 1(a). Ten micrometer-width air-gaps separate the different mechanical components, while an external silicon frame guarantees the anchoring of the four trapezoidal actuators. The total footprint of the device, comprising the 350 μm width of the external frame, is $4.5 \times 4.5\,\mathrm{mm}^2$. The first linear electro-mechanical vibration mode of the device occurs at 10.9 kHz and its eigenfunction is represented in Fig. 1(b).

III. LUMPED ELEMENT MODEL

The loudspeaker response is predicted by means of an equivalent electrical circuit, representing the multiphysics system composed of the electrical, mechanical, and

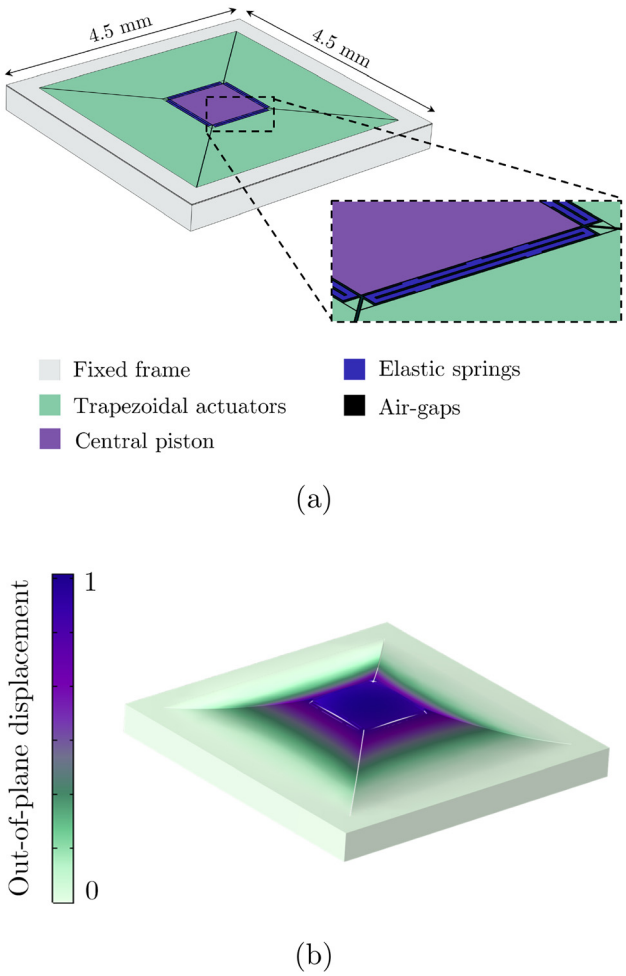

FIG. 1. (Color online) (a) Schematic view of the reference piezoelectric MEMS loudspeaker. A close-up view of the folded springs connecting trapezoidal plates hosting the PZT material with the central piston is reported for the sake of clarity. (b) Modal shape function of the first linear electro-mechanical resonant mode with contour of the normalized displacement field.

https://doi.org/10.1121/10.0024939

acoustical domains, as illustrated in Fig. 2(a). In the electrical domain, the effort and flow are voltage (V) and current (in A), respectively. The electrical and mechanical domains are coupled by a transformer that models the piezoelectric transduction mechanism of the MEMS loudspeaker. In the mechanical domain, the effort represents the force (in N) that actuates the vibrating diaphragm, while the flow represents the maximum velocity of the diaphragm (in m/s). The acoustical domain is coupled to the mechanical domain by the effective area S_{eff} of the loudspeaker. Thus, the effort and flow in the acoustical domain correspond to the pressure (in Pa) and volume velocity (in m^3/s), respectively.

The electrical domain is represented by a capacitance C_p; dielectric and leakage losses are here neglected. In the mechanical domain, the vibrating structure is modeled as a 1-degree-of-freedom mass-spring-damper system, where R_m, C_m, and M_m represent the first mode participating resistance, compliance, and mass of the moving diaphragm, respectively. The acoustical domain is composed of the acoustic impedance Z_a, depending on the loudspeaker acoustic load.

The maximum velocity of the loudspeaker can be derived as the ratio between the mechanical input force and the mechanical impedance seen from the electro-mechanical transducer:

$$v = \frac{F_{in}}{Z_m}, \tag{1}$$

where

$$Z_m = R_m + j\omega M_m + \frac{1}{j\omega C_m} + Z_a S_{eff}^2, \tag{2}$$

with ω the input circular frequency.

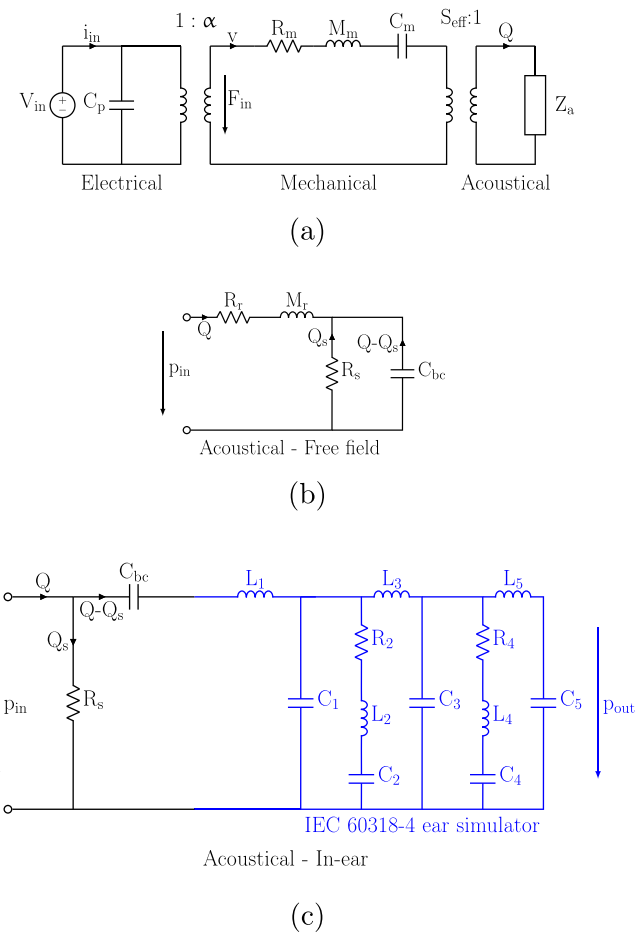

FIG. 2. (Color online) (a) Lumped equivalent network of the piezoelectric loudspeaker, composed of electrical, mechanical, and acoustical domains. (b) Acoustical domain for free-field conditions and (c) for in-ear conditions.

A. Equivalent circuit for free-field condition

The acoustic domain of the equivalent electrical circuit simulating the loudspeaker response in free-field conditions is reported in Fig. 2(b). The loudspeaker radiation in the unbounded front volume is represented by the lumped-elements R_r and M_r. The loudspeaker rear volume, i.e., *the* back chamber, is accounted for through the capacitor C_{bc}, placed in a parallel configuration with the resistor R_s, representing the viscous losses induced by air-gaps.

The partial acoustic short-circuit at low frequencies is induced by the presence of air-gaps, which put in connection the pressure fields in opposition of phase, generated by the front and rear sides of the speaker. The value of R_s affects the value of the net volume velocity $Q - Q_s$, which contributes to the output pressure. In the case of very narrow slits, and as a consequence of very high R_s, Q_s tends to zero. This means that the front volume and the back chamber of the speaker become acoustically decoupled and the acoustic short circuit is completely avoided. However, due to technological limitations, the air-gaps width is usually not sufficiently small to completely circumvent the acoustic short circuit.[9,21–23] For a correct prediction of the loudspeaker response, it is thus fundamental to include this phenomenon in the equivalent circuit.

The acoustic short-circuit depends on the flow Q_s, which can be computed by making use of the current divider formula:

$$Q_s = \frac{Q}{1 + j\omega C_{bc} R_s}. \tag{3}$$

Since Q_s is inversely proportional to the back chamber compliance C_{bc} and to the slit resistance R_s, for a fixed value of R_s, Q_s (and, as a consequence, the acoustic short-circuit) increases at decreasing back chamber compliance (see Sec. III D 2), and for a fixed value of C_{bc}, Q_s increases at decreasing slit resistance (see Sec. III D 3).

The acoustical equivalent impedance reads

$$Z_a = R_r + j\omega M_r + \frac{1}{j\omega C_{bc} + \frac{1}{R_s}}. \tag{4}$$

The loudspeaker maximum velocity v can be derived by substituting in Eq. (2) the expression of Z_a [Eq. (4)] and by considering that the input mechanical force F_{in} is given

by the product of the input voltage V_{in} and the piezoelectric transduction coefficient α:

$$v = \frac{\alpha V_{in}}{R_m + j\omega M_m + \frac{1}{j\omega C_m} + Z_a S_{eff}^2}. \tag{5}$$

For the computation of the sound pressure in free-field, the loudspeaker is treated as an equivalent piston element of area S_{eff}, flush mounted in an infinite baffle configuration. The sound pressure equation is retrieved from the loudspeaker effective volume velocity $(Q - Q_s)$ by exploiting the reduced Rayleigh's equation:[24]

$$p(r) = j\omega\rho_0(Q - Q_s)\frac{e^{-jk_0 r}}{2\pi r}, \tag{6}$$

where Q is given by multiplying Eq. (5) by S_{eff} and Q_s is given by Eq. (3). ρ_0 represents the air density, k_0 represents the wavenumber, and r is the distance between the loudspeaker and the evaluation point.

B. Equivalent circuit for in-ear condition

The equivalent circuit for in-ear condition is obtained by replacing the radiation impedance with the coupler input impedance [Fig. 2(c)]. The lumped equivalent network of the IEC 60318-4 ear-occluded simulator[25,26] is placed in a series configuration with the capacitor C_{bc}, representing the back chamber compliance. The electrical analog of the coupler main tube [see Fig. 1(a), right] is represented by a inductor-capacitor network transmission line, i.e., *the* components L_1, C_1, L_3, C_3, and L_5, C_5. The two electrical resistor-inductor-capacitor network circuits, with components R_2, L_2, C_2 and R_4, L_4, C_4, represent the coupler Helmholtz resonators, i.e., the coupler side volumes [Fig. 10(a), right]. The output pressure is obtained at the poles of capacitor C_5.

Also, for this configuration, the acoustic short-circuit depends on the leakage volume velocity Q_s, which determines the effective volume velocity Q–Q radiating in the coupler cavity.

From the equivalent network presented in Fig. 2(c), the equivalent acoustic impedance Z_a is

$$Z_a = \frac{1}{\frac{1}{R_s} + \frac{1}{\frac{1}{j\omega C_{bc}} + Z_{es}}}, \tag{7}$$

where Z_{es} represents the ear simulator input impedance, which can be expressed as

$$Z_{es} = j\omega L_1 + \frac{1}{j\omega C_1 + \frac{1}{Z_2} + \frac{1}{j\omega L_3 + \frac{1}{j\omega C_3 + \frac{1}{Z_4} + \frac{1}{Z_5}}}}, \tag{8}$$

with $Z_2 = j\omega L_2 + 1/j\omega C_2 + R_2$, $Z_4 = j\omega L_4 + 1/j\omega C_4 + R_4$ and $Z_5 = j\omega L_5 + 1/j\omega C_5$. The transfer function $T_a = p_{out}/p_{in}$ can be written as

$$T_a = \frac{Z_{es}}{\frac{1}{j\omega C_{bc}} + Z_{es}} T_{es}, \tag{9}$$

where T_{es} is the ear simulator transfer function, which can be expressed as

$$T_{es} = \frac{Z_{es} - j\omega L_1}{Z_{es}} \frac{\frac{1}{j\omega C_3 + \frac{1}{Z_4} + \frac{1}{Z_5}}}{j\omega L_3 + \frac{1}{j\omega C_3 + \frac{1}{Z_4} + \frac{1}{Z_5}}} \frac{1}{j\omega C_5 Z_5}. \tag{10}$$

The output pressure p_{out} can be retrieved from the velocity v [Eq. (1)] and the transfer function T_a:

$$p_{out} = T_a p_{in} = T_a Q Z_a = T_a S_{eff} v Z_a. \tag{11}$$

The parameters of the coupler equivalent circuit, listed in Table I, are derived from the classical low frequency approximation formulas for acoustic mass, compliance, and resistance,[25,27] considering the geometry of the G.R.A.S. RA0045 (Holte, Denmark) reported in Luan *et al.*[27]

The response of the sole coupler in terms of the absolute value of the acoustic transfer impedance normalized to the impedance at 500 Hz for a constant input volume displacement is shown by the solid line in Fig. 3. The amplification at high frequency is due to the half wavelength mode of the coupler main tube.

C. Electro-mechanical lumped-elements

By projecting the equations of motion on the first undamped electro-mechanical mode of the MEMS loudspeaker under study, the piezoelectric transduction coefficient α, the participating mass M_m, and the compliance C_m, can be derived, as schematized in Fig. 4. The mechanical resistance R_m represents instead the mechanical damping and can be estimated through numerical models or through

TABLE I. Equivalent circuit parameters of the IEC 60318-4 ear occluded simulator.

Parameter	Value	Unit
L_1	84.1	Pa s^2 m^{-3}
L_2	9722	Pa s^2 m^{-3}
L_3	128.1	Pa s^2 m^{-3}
L_4	1366	Pa s^2 m^{-3}
L_5	126.4	Pa s^2 m^{-3}
C_1	$9.83 \cdot 10^{-13}$	Pa m^{-3}
C_2	$1.76 \cdot 10^{-12}$	Pa m^{-3}
C_3	$1.5 \cdot 10^{-12}$	Pa m^{-3}
C_4	$1.85 \cdot 10^{-12}$	Pa m^{-3}
C_5	$1.48 \cdot 10^{-12}$	Pa m^{-3}
R_2	$5.72 \cdot 10^{7}$	Pa s m^{-3}
R_4	$8.23 \cdot 10^{7}$	Pa s m^{-3}

https://doi.org/10.1121/10.0024939

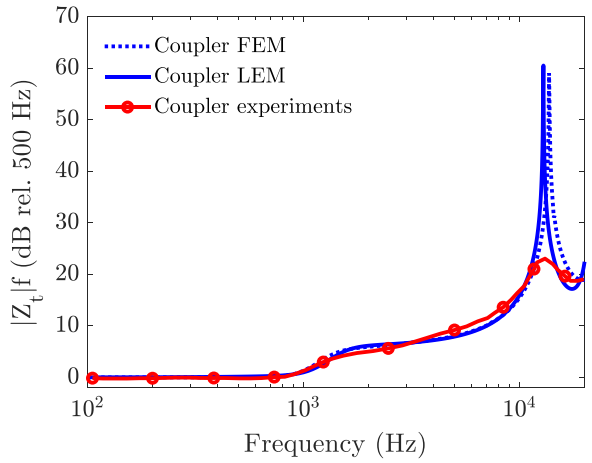

FIG. 3. (Color online) Comparison among the absolute value of the acoustic transfer impedance normalized to the impedance at 500 Hz of the LEM and FEM model of the ear simulator G.R.A.S. RA0045 and of the coupler G.R.A.S. RA0402 used in the experiments.

experiments, as will be done in Sec. V for the sake of simplicity.

To numerically compute the loudspeaker electro-mechanical mode, a modal analysis that considers as reference configuration the pre-deflected shape of the speaker induced by fabrication process pre-stresses and by the applied direct current (DC) voltage, is performed in COMSOL Multiphysics® v6.1 (Stockholm, Sweden). The pre-deflected configuration indeed defines the linearization point around which the dynamics occurs, as illustrated by Fig. 5, reporting the sound pressure level (SPL) curve for free-field conditions considering as linearization point the undeformed configuration (solid line) and the pre-deflected shape induced by a bias voltage of 12 V_{DC} and pre-stresses induced by the fabrication process (dotted line). The alternate voltage is set to 5 V_{pp}.

Under the hypothesis of linear piezoelectricity, the electro-mechanical constitutive model written in the so called *stress-charge* form is expressed as[28]

$$\boldsymbol{T} = \boldsymbol{C} : \boldsymbol{S} - \boldsymbol{e}^T \cdot \boldsymbol{E} = \boldsymbol{C} : \boldsymbol{S} + \boldsymbol{e}^T \cdot \nabla\phi \quad \textbf{in} \quad \Omega_p \tag{12}$$

$$\boldsymbol{D} = \boldsymbol{e} : \boldsymbol{S} + \boldsymbol{\varepsilon} \cdot \boldsymbol{E} = \boldsymbol{e} : \boldsymbol{S} - \boldsymbol{\varepsilon} \cdot \nabla\phi \quad \textbf{in} \quad \Omega_p, \tag{13}$$

where Ω_p is the piezoelectric domain, $\boldsymbol{T}$ is the second-order stress tensor, $\boldsymbol{S}$ is the second-order strain tensor, and $\boldsymbol{C}$ is the fourth-order elastic stiffness tensor at constant $\boldsymbol{E}$. $\boldsymbol{D}$ is the electric displacement, $\boldsymbol{\varepsilon}$ is the second-order dielectric permittivity tensor at constant $\boldsymbol{S}$, and $\boldsymbol{e}$ is the third-order piezoelectric coupling tensor. Lastly, $\boldsymbol{E}$ is the electric field and $\nabla\phi$ is the voltage difference.

If thin piezoelectric layers and high electric fields (on the order of 10^7 V/m for actuating voltages in the range 0–30 V) are considered as in the present case, the one-way formulation[29] of the piezoelectric constitutive law can be employed. That means that the effect of the mechanical strains on the electric displacement (direct piezoelectric effect) is neglected. The piezoelectric constitutive equations then become

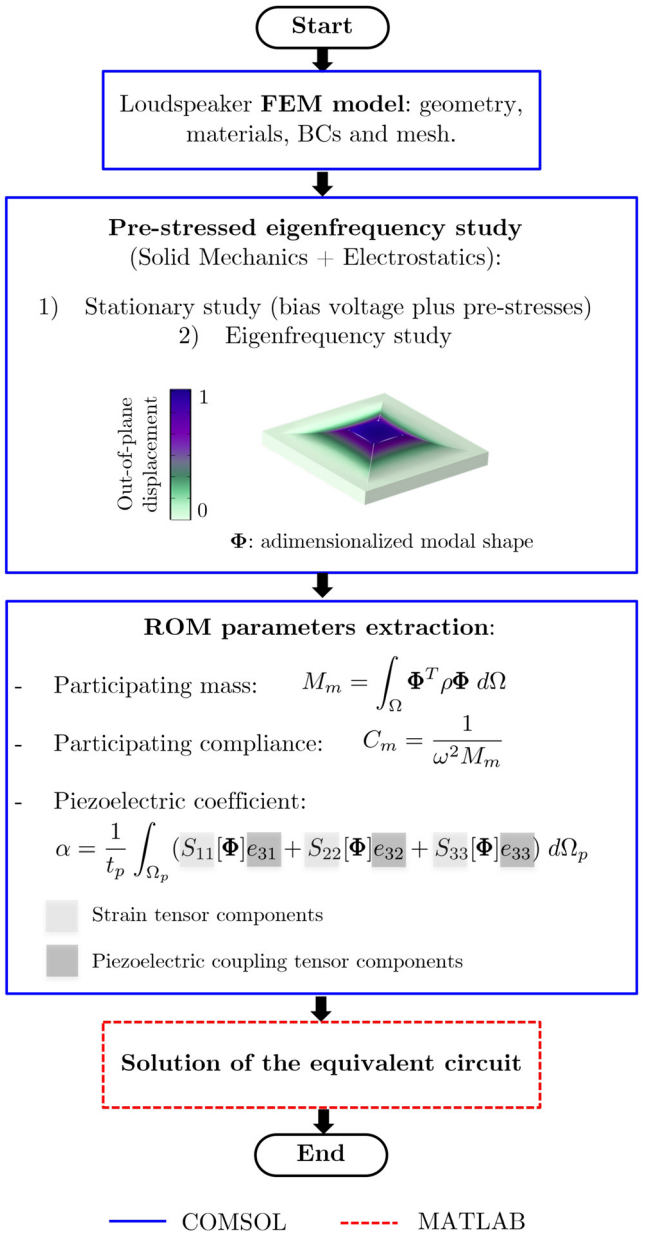

FIG. 4. (Color online) Flowchart for the extraction of the electro-mechanical parameters. The FEM software is COMSOL Multiphysics® v6.1 and the equivalent circuit is implemented in MATLAB R2022a (Natick, MA). BCs, boundary conditions. ROM, reduced order model.

$$\boldsymbol{T} = \boldsymbol{C} : \boldsymbol{S} - \boldsymbol{e}^T \cdot \boldsymbol{E} = \boldsymbol{C} : \boldsymbol{S} + \boldsymbol{e}^T \cdot \nabla\phi \quad \textbf{in} \quad \Omega_p, \tag{14}$$

$$\boldsymbol{D} = \boldsymbol{\varepsilon} \cdot \boldsymbol{E} = -\boldsymbol{\varepsilon} \cdot \nabla\phi \quad \textbf{in} \quad \Omega_p. \tag{15}$$

By exploiting the virtual work principle in the material form, the restricted weak formulation of the equations of motion becomes

$$\int_\Omega \rho \ddot{\boldsymbol{u}} \cdot \tilde{\boldsymbol{u}}\, d\Omega + \int_\Omega \boldsymbol{T} : \boldsymbol{S}[\tilde{\boldsymbol{u}}]\, d\Omega = 0 \quad \forall \tilde{\boldsymbol{u}} \in C_u(0), \tag{16}$$

where ρ is the material density, $\mathbf{u}$ is the displacement field, $\ddot{\boldsymbol{u}}$ is the acceleration field, $\tilde{\boldsymbol{u}}$ is a suitable test function belonging to the space $C_u(0)$, that is, the space of functions

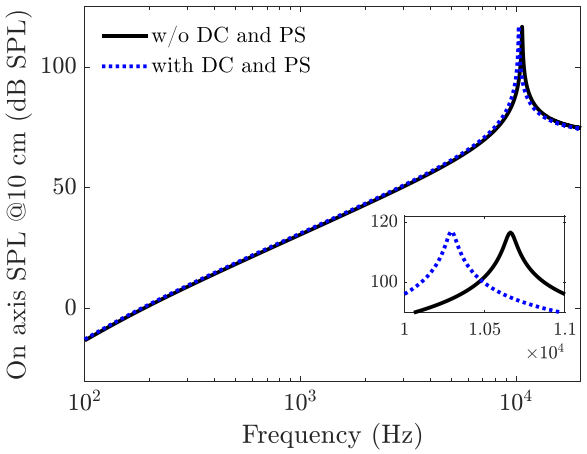

FIG. 5. (Color online) SPL curve for free-field conditions considering as linearization point the undeformed configuration (solid line) and the pre-deflected shape induced by a bias voltage of $12\,V_{DC}$ and pre-stresses induced by the fabrication process (dotted line). A zoom of the resonance region is reported in the inset.

that vanish on the boundary where Dirichlet boundary conditions are prescribed.

By substituting the constitutive law in Eq. (16) and by moving known quantities to the right-hand-side of the equation, the following expression is obtained:

$$\int_\Omega \rho\ddot{\boldsymbol{u}}\cdot\tilde{\boldsymbol{u}}\,d\Omega+\int_\Omega \boldsymbol{S}[\tilde{\boldsymbol{u}}]:\boldsymbol{C}:\boldsymbol{S}[\boldsymbol{u}]\,d\Omega = \int_{\Omega_p}\boldsymbol{S}[\tilde{\boldsymbol{u}}]:(\boldsymbol{e}^{\boldsymbol{T}}\cdot\boldsymbol{E})\,d\Omega \quad \forall\tilde{\boldsymbol{u}}\in C_u(0). \tag{17}$$

By considering a piezoelectric thin film, the electric field generated by a voltage difference across its thickness t_p can be expressed as $\boldsymbol{E}=E\boldsymbol{e_3}=(V_{in}/t_p)\boldsymbol{e_3}$, where $\boldsymbol{e_3}$ represents the versor of the out-of-plane z axis. Hence, the right-hand-side of Eq. (17) reduces to

$$E\int_{\Omega_p}(S_{11}[\tilde{\boldsymbol{u}}]e_{31}+S_{22}[\tilde{\boldsymbol{u}}]e_{32}+S_{33}[\tilde{\boldsymbol{u}}]e_{33})\,d\Omega. \tag{18}$$

The mechanical eigenmode $\boldsymbol{\Phi}$ of the speaker under study, adimensionalized with unit maximum displacement, is then employed as test function $\tilde{\boldsymbol{u}}$ to obtain the ROM. Physical displacement, velocity, and acceleration then are written as

$$\tilde{\boldsymbol{u}}(\boldsymbol{x})=\boldsymbol{\Phi}(\boldsymbol{x}), \tag{19}$$

$$\boldsymbol{u}(\boldsymbol{x},t)=\boldsymbol{\Phi}(\boldsymbol{x})q(t), \tag{20}$$

$$\dot{\boldsymbol{u}}(\boldsymbol{x},t)=\boldsymbol{\Phi}(\boldsymbol{x})\dot{q}(t), \tag{21}$$

$$\ddot{\boldsymbol{u}}(\boldsymbol{x},\boldsymbol{t})=\boldsymbol{\Phi}(\boldsymbol{x})\ddot{q}(t), \tag{22}$$

where $q(t)$ represents the modal coordinate. The corresponding 1-degree-of-freedom equation can be written as

$$\ddot{q}(t)\int_\Omega \boldsymbol{\Phi}^T\rho\boldsymbol{\Phi}\,d\Omega+q(t)\int_\Omega \boldsymbol{S}[\boldsymbol{\Phi}]:\boldsymbol{C}:\boldsymbol{S}[\boldsymbol{\Phi}]\,d\Omega = E\int_{\Omega_p}(S_{11}[\boldsymbol{\Phi}]e_{31}+S_{22}[\boldsymbol{\Phi}]e_{32}+S_{33}[\boldsymbol{\Phi}]e_{33})\,d\Omega, \tag{23}$$

where the modal mass, the modal compliance, and the piezoelectric transduction factor can be identified through

$$M_m\ddot{q}(t)+\frac{1}{C_m}q(t)=F_{in}=E\gamma=\frac{V}{t_p}\gamma=V_{in}\alpha. \tag{24}$$

Assuming an harmonic excitation and recasting the equation of motion in terms of velocity, Eq. (24) becomes

$$j\omega M_m\dot{q}+\frac{1}{j\omega C_m}\dot{q}=V_{in}\alpha. \tag{25}$$

The current v which flows in the mechanical domain of the circuit is the maximum speaker velocity. The velocity profile in the whole speaker domain can then be easily reconstructed through Eq. (21).

In practical terms, the quantities derived in COMSOL Multiphysics® are the first eigenvector $\boldsymbol{\Phi}$, the corresponding eigenvalue ω_0^2, and the strain components $S_{11}(\boldsymbol{\Phi})$, $S_{22}(\boldsymbol{\Phi})$, and $S_{33}(\boldsymbol{\Phi})$. M_m is computed through the first integral term of Eq. (23), $C_m=1/(M_m\omega_0^2)$, and α is obtained by integrating on the piezoelectric domain the linear combination of the strain components and the piezoelectric coefficients [right-hand-side of Eq. (23)].

The effective area S_{eff} used to couple the mechanical and the acoustical domains is computed starting from the definition of the volume velocity as

$$Q=\int_{\partial\Omega_f}\dot{\boldsymbol{u}}\cdot\boldsymbol{n}\,dS=\dot{q}\int_{\partial\Omega_f}\boldsymbol{\Phi}\cdot\boldsymbol{n}\,dS=vS_{eff}, \tag{26}$$

where $\partial\Omega_f$ is the surface area of the front side of the speaker and $\boldsymbol{n}$ its outward normal.

The piezoelectric capacitance C_p is finally computed by considering the standard formula for parallel plate capacitors:[28]

$$C_p=\frac{\varepsilon_r\varepsilon_0 A_p}{t_p}, \tag{27}$$

where ε_r is the relative permittivity of the dielectric material, ε_0 the vacuum permittivity, and A_p is the area where piezoelectric material is present.

The electro-mechanical lumped parameters of the speaker under investigation are reported in Table II.

D. Acoustical lumped-elements

The acoustical lumped-elements R_r, M_r, C_{bc}, and R_s are derived through analytical formulas.

TABLE II. Electro-mechanical lumped-elements corresponding to the reference MEMS loudspeaker.

Parameter	Value	Unit
C_p	68	nF
α	$4.63\cdot10^{-4}$	N/V
C_m	$2.25\cdot10^{-3}$	m/N
M_m	$9.85\cdot10^{-8}$	kg
S_{eff}	$3.93\cdot10^{-6}$	m^2

https://doi.org/10.1121/10.0024939

1. Radiation impedance

The microspeaker radiation impedance is obtained by considering a rigid plate, flush-mounted into an infinite baffle:[30]

$$Z_r = Z_c(R + jX), \tag{28}$$

where Z_c represents the characteristic acoustic impedance of air at ambient temperature equal to $\rho_0 c_0/S_{eff}$. The R and X components of Z_r depend on the assumed plate shape. Considering the audio frequency range and the reference loudspeaker characteristic dimension, the radiation impedance of a square plate[30] and of a circular plate of the same surface area are practically superimposed, as demonstrated in Fig. 6 and as already discussed in the work of Liechti *et al.*[20] For the sake of simplicity, the radiation impedance of a circular plate is considered in the model:[24]

$$R(x) = 1 - \frac{2J_1(x)}{x} = \frac{x^2}{2\cdot 4} - \frac{x^4}{2\cdot 4^2\cdot 6} + \frac{x^6}{2\cdot 4^2\cdot 6^2\cdot 8} - o(x^8), \tag{29}$$

$$X(x) = \frac{2H_1(x)}{x} = \frac{4}{\pi}\left(\frac{x}{3} - \frac{x^3}{3^2\cdot 5} + \frac{x^5}{3^2\cdot 5^2\cdot 7} - o(x^7)\right), \tag{30}$$

where $J_1(x)$ is the first order Bessel function and $H_1(x)$ is the first order Struve function. The piston radius a is derived from the speaker effective area as $a = \sqrt{S_{eff}/\pi}$.

In the low-frequency limit ($k_0 a \ll 1$), the radiation impedance can be approximated by the first term of the power expansion. The radiation resistance reduces to

$$R_r = \frac{1}{2} Z_c (k_0 a)^2, \tag{31}$$

and the radiation reactance is written as

$$X_r = \frac{8}{3\pi} Z_c k_0 a. \tag{32}$$

Given the microspeaker dimensions, the low frequency approximation is acceptable in the whole audible range, as illustrated in Fig. 6. In the equivalent circuit, the radiation impedance is then represented by a resistor of resistance R_r and with an inductor of inductance $M_r = X_r/\omega = 8\rho_0 a/3\pi S_{eff}$, which translates into a loudspeaker added damping and mass, respectively.

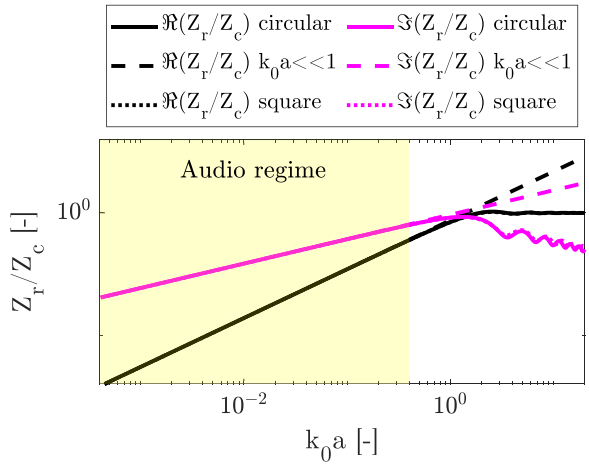

FIG. 6. (Color online) Comparison of the real and imaginary part of the radiation impedance for a circular rigid plate, a square rigid plate, and assuming the low frequency approximation ($k_0 a \ll 1$). The audible frequency range is evidenced through the shaded area.

2. Back chamber

The main effect of the back chamber is a stiffening of the loudspeaker, represented in the equivalent circuit through the compliance C_{bc} that can be evaluated as[31]

$$C_{bc} = \frac{V_{bc}}{\rho_0 c_0^2}, \tag{33}$$

where V_{bc} is the back chamber volume and c_0 is the speed of sound in air.

Figure 7 shows the pressure radiated by the reference loudspeaker for an actuating voltage of 12 V_{DC} plus 5 V_{pp} at varying back chamber volume. In particular, the selected volumes of 0.007 cm^3, 0.022 cm^3, 0.100 cm^3, 1 cm^3, and 10 cm^3 correspond to back chamber stiffnesses equal to 65%, 20%, 5%, 0.5%, and 0.05% of the speaker stiffness, respectively.

Small volumes shift the speaker resonance frequency to higher frequencies, thus worsening the low frequency response. For volume values greater than 1 cm^3, the back chamber stiffening effect can be considered negligible. This consideration guided the choice of the package exploited for experimental tests sketched in Fig. 8(a). The experimental back volume is composed of a small chamber of 0.006 cm^3 connected through a tube to a chamber of 1 cm^3 volume. The corresponding equivalent network is reported in Fig. 8(b), where $C_{bc,1}$ is computed through Eq. (33), $L_{bc} = \rho_0 L/S$, with L being the tube length and S its surface area, and $Z_{bc,2}$ being the input impedance of the bigger back chamber. The latter is expressed as

$$Z_{bc,2} = -j\frac{\rho_0 c_0}{S_{bc,2}} \cot(k_0 l_{bc,2}), \tag{34}$$

where $S_{bc,2}$ is the back cavity surface area and $l_{bc,2}$ is its height.

The input impedance of the whole back cavity can be expressed as

$$Z_{in} = \frac{1}{j\omega C_{bc,1} + \dfrac{1}{j\omega L_{bc} + Z_{bc,2}}}, \tag{35}$$

whose first resonance occurs at 20.1 kHz in correspondence of the half wavelength resonance of the chamber.

3. Air-gaps damping

The lumped-element R_s introduced in the speaker equivalent circuit represents the losses that occur inside the

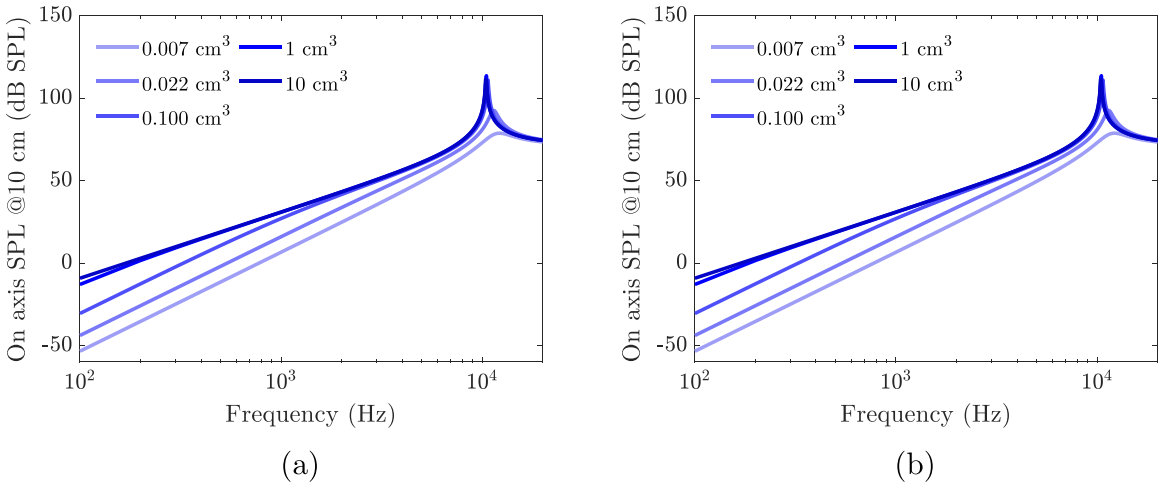

FIG. 7. (Color online) Sound pressure level radiated by the piezoelectric MEMS speaker in (a) free-field and (b) in-ear conditions at varying back chamber volume and setting the air-gaps width to 10 μm.

slits due to the air viscosity, μ. The resistance value for a single rectangular slit can be deduced by considering the reduced Navier–Stokes equation for a Poiseuille flow[32] and is expressed as

$$R_s = \frac{12\mu t_{pl}}{l_s w_s^3}, \tag{36}$$

where t_{pl} is the out-of-plane thickness of the speaker, l_s is the length of the slit, and w_s is its width.

The speaker geometry is usually characterized by a set of multiple air-gaps.[10,11] Considering n slits, the total resistance is written as

$$R_s = \frac{1}{\frac{1}{R_1} + \cdots + \frac{1}{R_n}}, \tag{37}$$

given the different air-gaps in a parallel configuration.

The SPL response at varying air-gaps width, for an actuation voltage of 12 V_{DC} plus 12 V_{pp} and a back chamber of volume equal to 1 cm^3, is reported in Fig. 9 for free-field and in-ear conditions. With increasing air-gaps width, the acoustic-short circuit becomes increasingly more impactful, worsening the low frequency response. For air-gaps width of 10 μm, like those present in the reference speaker to cope with fabrication process constraints, the acoustic short-circuit affects the response for frequencies below 500 Hz only.

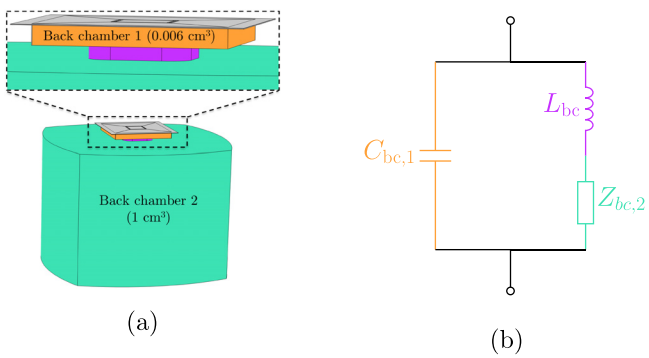

FIG. 8. (Color online) (a) Geometry of the back chamber employed in the experimental tests and (b) corresponding equivalent circuit.

IV. FULL-FEM MODEL

The equivalent circuit predictions in terms of SPL are compared with those of a full-FEM electro-mechano-acoustic FEM implemented in COMSOL Multiphysics® [Fig. 10(a)]. The numerical model takes into account *(i)* the elasto-dynamic behaviour of the mechanical structure, *(ii)* the electro-mechanical coupling through the piezoelectric constitutive law, *(iii)* the mechano-acoustic coupling between the mechanical structure and the acoustic domains on the front and rear sides of the speaker, *(iv)* the boundary layer induced by the viscous properties of the air in the narrow gaps through the low reduced frequency formulation.[33,34] For free-field conditions, the radiation in unbounded domain is implemented through a perfectly matched layer to reproduce the Sommerfeld radiation boundary condition. The in-ear condition is simulated through the ear simulator G.R.A.S. RA0045,[27] whose adimensionalized transfer impedance under a constant input volume displacement is represented in Fig. 3 (dotted line).

The SPL curves derived with the FEM model are depicted with dotted lines in Fig. 10(b) for free-field conditions and in Fig. 10(c) for in-ear conditions. When compared with reported LEM predictions [Fig. 10(b), solid line], a very good agreement in the whole frequency range is demonstrated. The comparison is extended up to 25 kHz to also highlight the half wavelength resonance of the back cavity mentioned in Sec. III D 2.

V. EXPERIMENTAL CHARACTERIZATION

For in-ear conditions, the SPL evaluated through the proposed equivalent circuit is also compared with experimental measurements carried out on six prototypes of the

https://doi.org/10.1121/10.0024939

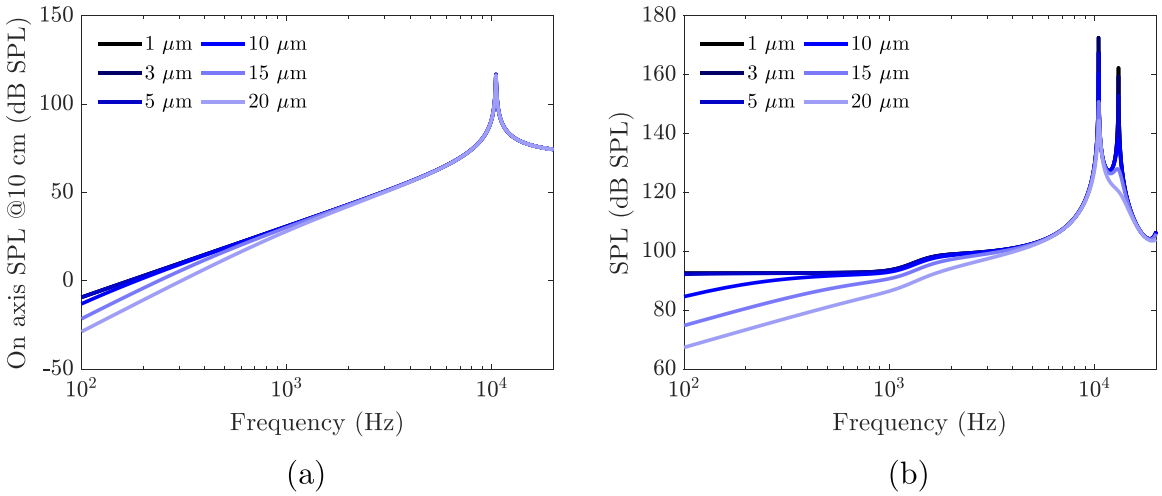

FIG. 9. (Color online) Sound pressure level radiated by the piezoelectric MEMS speaker in (a) free-field and (b) in-ear conditions at varying air-gaps width and setting the back chamber volume to 1 cm^3.

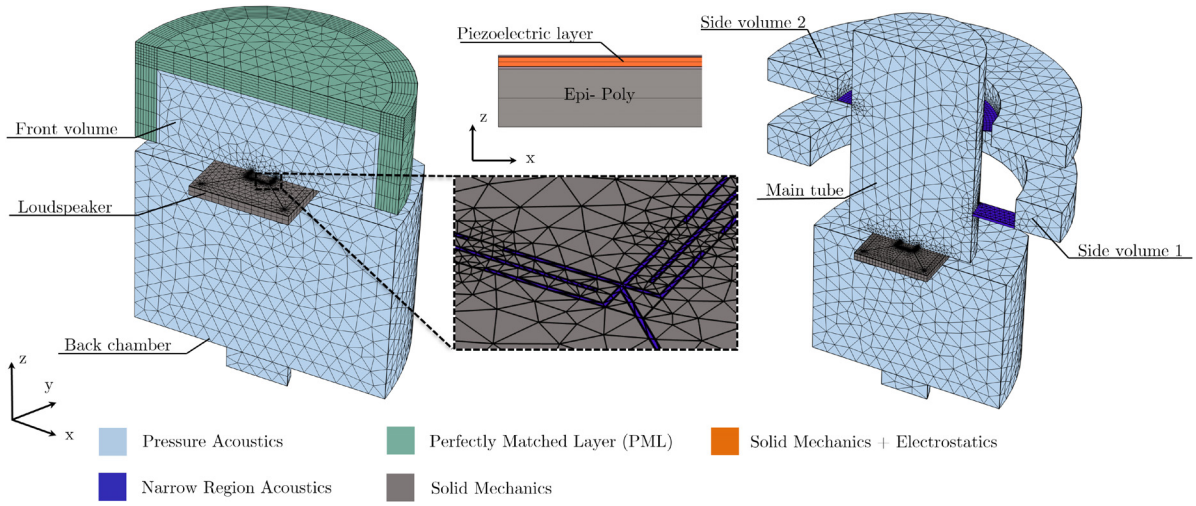

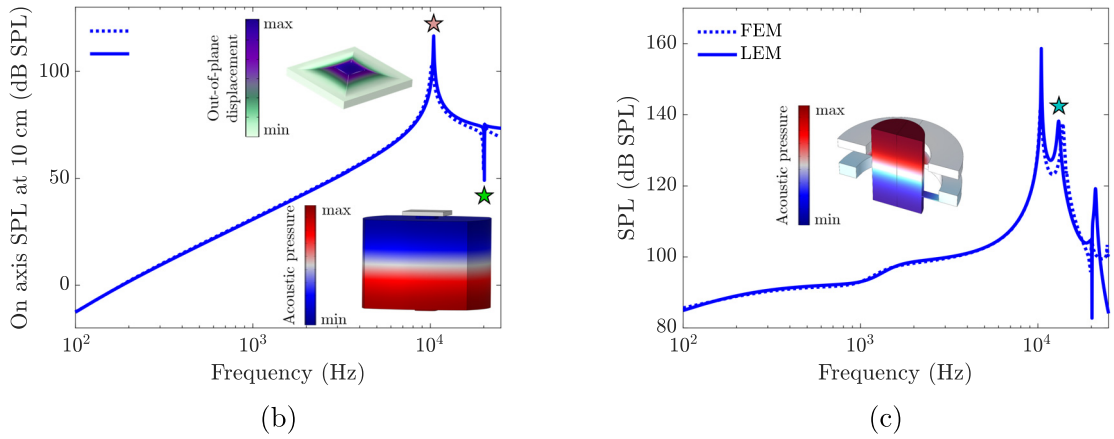

FIG. 10. (Color online) (a) FEM model implemented in COMSOL Multiphysics® for free-field (left) and in-ear conditions (right). Comparison between SPL predictions of the equivalent circuit (solid line) and of the FEM model (dotted line) for a bias voltage of 12 V_{DC} plus an alternating voltage of 5 V_{pp}, for (b) free-field and (c) in-ear conditions. The insets report (b) the loudspeaker deformed shape at its resonance frequency, the acoustic pressure distribution at the half wavelength resonance of the back chamber, and (c) of the ear simulator.

reference speaker, fabricated by STMicroelectronics (Cornaredo, Italy). For experimental tests, the device is mounted on a custom printed circuit board (PCB) and coupled with an acrylonitrile butadiene styrene (ABS) thermoplastic package composed of a back chamber of 1 cm^3 and a front adapter of 1 mm height to connect the speaker with the ear simulator [Fig. 11(a)].

The experimental setup includes the anechoic chamber G.R.A.S. AL0030-S2, the ear simulator G.R.A.S. RA0402, together with microphone G.R.A.S. 46 BD 1/4. The audio analyzer (APx525) allows us to generate DC and alternating current (AC) signals for the MEMS actuation and to convert the signal from the microphone into SPL data [Fig. 11(b)]. All the measurements reported in the following refer to a DC voltage of 12 V_{DC}, which is the maximum bias voltage that can be generated by the employed audio analyzer. As it is well known, to limit piezoelectric domains re-orientation and hence hysteresis, the piezoelectric actuation is usually performed by adding an offset equal to at least half of the input dynamic, avoiding the change of sign of the electric field.[35] Measurements at 30 V_{pp} are, however, reported here, assuming that the small negative difference does not significantly affect the response of the speaker.

To match the quality factor of the half wavelength resonance of the G.R.A.S. RA0402[36] (solid line with circles in Fig. 3), three additional resistances $R_1 = 2.36 \cdot 10^{-6}$ Pa s m^{-3}, $R_3 = 3.60 \cdot 10^{-6}$ Pa s m^{-3}, and $R_5 = 3.55 \cdot 10^{-6}$ Pa s m^{-3} are introduced in the equivalent circuit of the ear simulator in series to the acoustic masses L_1, L_3, and L_5, respectively. The value of R_m has also been tuned by considering a mechanical Q_m factor of 10, to match the peak amplitude of the speaker resonance frequency of the experimental SPL curve.

The SPL curves measured on six protorypes for a DC voltage of 12 V_{DC} and an AC voltage of 5 V_{pp} and 30 V_{pp} are reported in Figs. 11(c) and 11(d), respectively. The mean experimental value of the six measurements is reported with a solid line with circles and the standard deviation is indicated by the shaded area. For the measurement at 30 V_{pp}, the acquisition is stopped at 10 kHz to avoid the

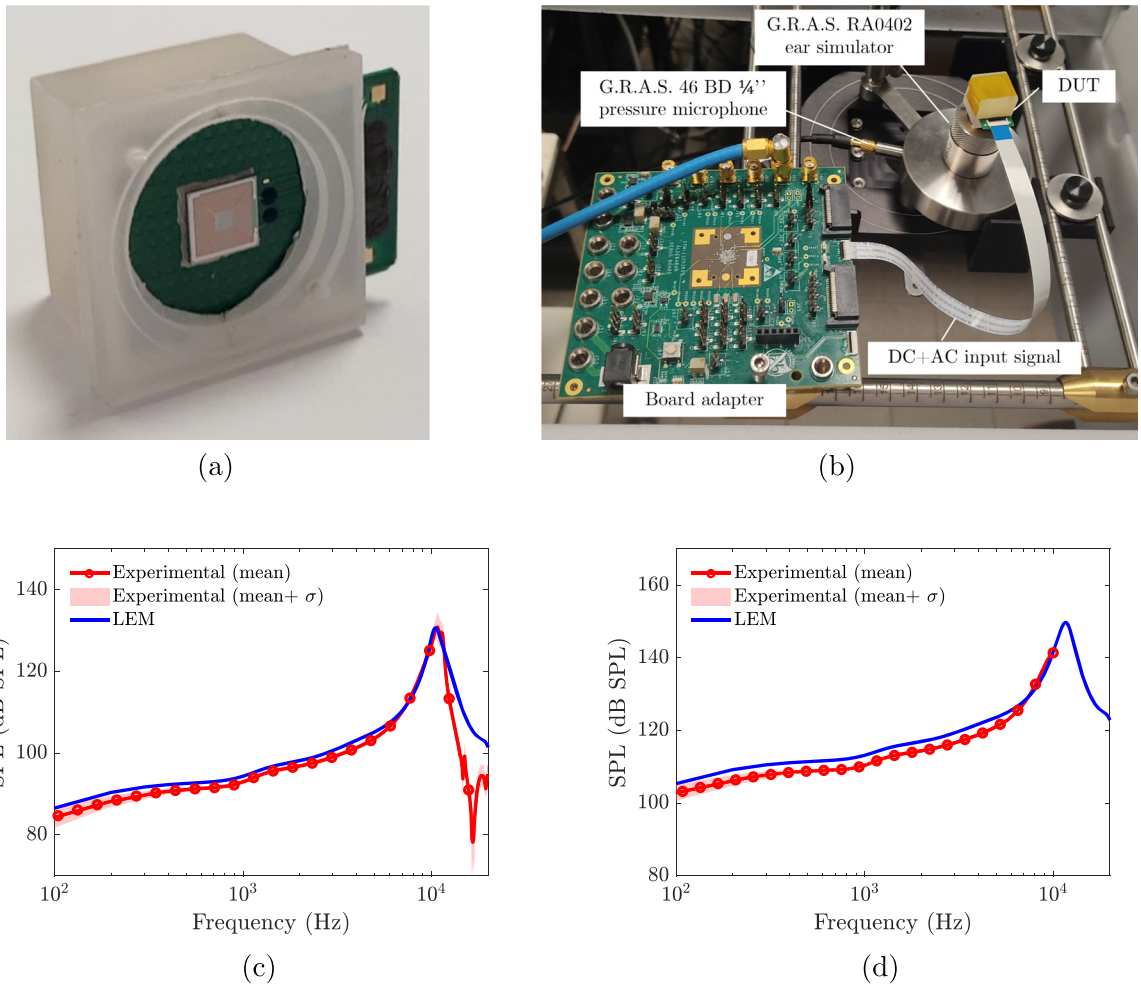

FIG. 11. (Color online) (a) Fabricated microspeaker mounted on a custom PCB and coupled with the package for in-ear acoustic tests. (b) Acoustic measurement setup composed of the audio analyzer (AP × 525), the ear simulator G.R.A.S. RA0402 together with the $\frac{1}{4}$ in. microphone G.R.A.S. 46 BD Comparison between theoretical (solid curve) and experimental (mean value in solid line with circles and standard deviation in shaded area) SPL frequency spectra for a bias voltage of 12 V_{DC} plus (c) 5 V_{pp} and (d) 30 V_{pp}. In the latter case, the acquisition is stopped at 10 kHz to avoid the breakup of the prototypes.

breakup of the prototypes. Note that the added damping makes the two resonance peaks merge into one.

Overall, the theoretical vs experimental matching is very good up to 10 kHz, the range in which the ear simulator is able to accurately reproduce the acoustical behaviour of the ear canal.[37]

The antiresonance that appears at high frequency is due to an unwanted activation of a rotational mode of the loudspeaker, caused by a small asymmetry in the springs connecting the trapezoidal actuators and the central piston, induced by fabrication process imperfections.

VI. CONCLUSION

A lumped-parameters equivalent circuit based on a ROM of the electro-mechanical problem is proposed as a fast and accurate modeling of piezoelectric MEMS speakers. The FEM-assisted extraction of the electro-mechanical parameters allows us to account for arbitrarily complex geometries and to consider the shift in the speaker resonance frequency due to an initial non-null pre-deflected configuration. The acoustic short-circuit between the speaker front and rear sides induced by the presence of air-gaps is also taken into account by the proposed equivalent circuit. The very good matching in terms of SPL among the equivalent circuit predictions, FEM simulations. and experimental data demonstrates the ability of the proposed method to accurately simulate the speaker performance—thus representing a fast tool for the design of this class of MEMS speakers.

Future perspectives are related to the extension of the proposed equivalent circuit to the nonlinear regime with the inclusion of the piezoelectric hysteretical behaviour and geometric nonlinearities for the estimation of total harmonic distortion (THD).

ACKNOWLEDGMENTS

The authors thank STMicroelectronics for the fabrication of the prototypes and, in particular, Fabrizio Cerini and Silvia Adorno for their precious contribution to the experimental tests.

AUTHOR DECLARATIONS

Conflict of Interest

The authors have no conflicts to disclose.

DATA AVAILABILITY

The data that support the findings of this study are available from the first author upon reasonable request.

[1]A. Gemelli, M. Tambussi, S. Fusetto, A. Aprile, E. Moisello, E. Bonizzoni, and P. Malcovati, "Recent trends in structures and interfaces of MEMS transducers for audio applications: A review," Micromachines **14**(4), 847 (2023).
[2]A. Rusconi, S. Costantini, and C. Prelini, "Micro speakers," in *Silicon Sensors and Actuators* (Springer, Cham, Switzerland, 2022), pp. 651–676.
[3]D. Beer, A. Mannchen, T. Fritsch, J. Kuller, A. Zhykhar, G. Fischer, and F. M. Fiedler, "Expedition MEMS speaker," Forum Acusticum, December 2020, Lyon, France, pp. 2921–2928.
[4]H. Wang, Y. Ma, Q. Zheng, K. Cao, Y. Lu, and H. Xie, "Review of recent development of MEMS speakers," Micromachines **12**(10), 1257 (2021).
[5]R. Liechti, S. Durand, T. Hilt, F. Casset, C. Dieppedale, and M. Colin, "High performance piezoelectric MEMS loudspeaker based on an innovative wafer bonding process," Sens. Actuators A: Phys. **358**, 114413 (2023).
[6]H. Wang, Z. Chen, and H. Xie, "A high-SPL piezoelectric MEMS loud speaker based on thin ceramic PZT," Sens. Actuators A: Phys. **309**, 112018 (2020).
[7]M. V. Garud and R. Pratap, "A novel MEMS speaker with peripheral electrostatic actuation," J. Microelectromech. Syst. **29**(4), 592–599 (2020).
[8]I. Shahosseini, E. Lefeuvre, J. Moulin, E. Martincic, M. Woytasik, and G. Lemarquand, "Optimization and microfabrication of high performance silicon-based MEMS microspeaker," IEEE Sens. J. **13**(1), 273–284 (2013).
[9]F. Stoppel, A. Männchen, F. Niekiel, D. Beer, T. Giese, and B. Wagner, "New integrated full-range MEMS speaker for in-ear applications," in *2018 IEEE Micro Electro Mechanical Systems (MEMS)*, Belfast, Ireland (2018), pp. 1068–1071.
[10]C. Gazzola, V. Zega, F. Cerini, S. Adorno, and A. Corigliano, "On the design and modeling of a full-range piezoelectric MEMS loudspeaker for in-ear applications," J. Microelectromech. Syst. **32**, 626–637 (2023).
[11]T.-C. Wei, Z.-S. Hu, S.-W. Chang, and W. Fang, "On the design of piezoelectric MEMS microspeaker with high fidelity and wide bandwidth," in *2023 IEEE 36th International Conference on Micro Electro Mechanical Systems (MEMS)* (IEEE, Munich, Germany, 2023), pp. 127–130.
[12]Y.-C. Chen, H.-H. Cheng, M.-C. Cheng, S.-C. Lo, C.-K. Chan, and W. Fang, "On the design of a two-way piezoelectric MEMS microspeaker based on a multi-shape cantilever array for high-frequency applications," J. Micromech. Microeng. **33**(7), 074001 (2023).
[13]C. Gazzola, V. Zega, A. Corigliano, P. Lotton, and M. Melon, "Lumped-parameters equivalent circuit for piezoelectric MEMS speakers modeling," Forum Acusticum, 2023, Torino, Italy.
[14]S.-H. Tseng, S.-C. Lo, Y.-J. Wang, S.-W. Lin, M. Wu, and W. Fang, "Sound pressure and low frequency enhancement using novel PZT MEMS microspeaker design," in *2020 IEEE 33rd International Conference on Micro Electro Mechanical Systems (MEMS)*, Vancouver, BC, Canada (2020), pp. 546–549.
[15]Y. Ma, Y. Lu, N. Deng, Q. Zheng, K. Cao, H. Wang, and H. Xie, "A PZT MEMS loudspeaker with a quasi-closed diaphragm," Sens. Actuators A: Phys. **358**, 114454 (2023).
[16]L. Xu, M. Sun, M. Zhang, C. Liu, X. Yang, and W. Pang, "A piezoelectric MEMS speaker with stretchable film sealing," in *2023 IEEE 36th International Conference on Micro Electro Mechanical Systems (MEMS)* (IEEE, Munich, Germany, 2023), pp. 673–676.
[17]J. H. Huang, H.-C. Her, Y. Shiah, and S.-J. Shin, "Electroacoustic simulation and experiment on a miniature loudspeaker for cellular phones," J. Appl. Phys. **103**(3), 033502 (2008).
[18]B. Kaiser, H. A. G. Schenk, L. Ehrig, F. Wall, J. M. Monsalve, S. Langa, M. Stolz, A. Melnikov, H. Conrad, D. Schuffenhauer, and H. Schenk, "The push-pull principle: An electrostatic actuator concept for low distortion acoustic transducers," Microsyst. Nanoeng. **8**(1), 125 (2022).
[19]B. Kaiser, S. Langa, L. Ehrig, M. Stolz, H. Schenk, H. Conrad, H. Schenk, K. Schimmanz, and D. Schuffenhauer, "Concept and proof for an all-silicon MEMS micro speaker utilizing air chambers," Microsyst. Nanoeng. **5**(1), 43 (2019).
[20]R. Liechti, S. Durand, T. Hilt, F. Casset, C. Dieppedale, T. Verdot, and M. Colin, "A piezoelectric MEMS loudspeaker for in-ear and free field applications lumped and finite element models," Microelectron. Rel. **134**, 114555 (2022).
[21]C. Gazzola, V. Zega, F. Cerini, S. Adorno, and A. Corigliano, "A mechanically-open and acoustically-closed piezo-MEMS speaker for in-ear applications," in *2023 22nd International Conference on Solid-State Sensors, Actuators and Microsystems (Transducers)*, Kyoto, Japan (IEEE, New York, 2023).
[22]F. Stoppel, C. Eisermann, S. Gu-Stoppel, D. Kaden, T. Giese, and B. Wagner, "Novel membrane-less two-way MEMS loudspeaker based on piezoelectric dual-concentric actuators," in *2017 19th International Conference on Solid-State Sensors, Actuators and Microsystems (TRANSDUCERS)* (IEEE, Kaohsiung, Taiwan, 2017), pp. 2047–2050.

[23]H.-H. Cheng, S.-C. Lo, Z.-R. Huang, Y.-J. Wang, M. Wu, and W. Fang, "On the design of piezoelectric MEMS microspeaker for the sound pressure level enhancement," Sens. Actuators A: Phys. **306**, 111960 (2020).
[24]L. E. Kinsler, A. R. Frey, A. B. Coppens, and J. V. Sanders, *Fundamentals of Acoustics* (John Wiley & Sons, New York, 2000).
[25]L. Nielsen, A. Schuhmacher, B. Liu, and S. Jonsson, "Simulation of the IEC 60711 occluded ear simulator," in *Audio Engineering Society Convention 116*, Berlin, Germany (Audio Engineering Society, New York, 2004).
[26]R. Liechti, S. Durand, T. Hilt, F. Casset, C. Poulain, G. Le Rhun, F. Pavageau, H. Kuentz, and M. Colin, "Total harmonic distortion of a piezoelectric MEMS loudspeaker in an IEC 60318-4 coupler estimation using static measurements and a nonlinear state space model," Micromachines **12**(12), 1437 (2021).
[27]Y. Luan, F. Sgard, S. Benacchio, H. Nélisse, and O. Doutres, "A transfer matrix model of the IEC 60318-4 ear simulator: Application to the simulation of earplug insertion loss," Acta Acust. united Acust. **105**(6), 1258–1268 (2019).
[28]A. Corigliano, R. Ardito, C. Comi, A. Frangi, A. Ghisi, and S. Mariani, *Mechanics of Microsystems* [John Wiley & Sons (UK) Ltd., Croydon, UK, 2018].
[29]A. Frangi, A. Opreni, N. Boni, P. Fedeli, R. Carminati, M. Merli, and G. Mendicino, "Nonlinear response of PZT-actuated resonant micromirrors," J. Microelectromech. Syst. **29**(6), 1421–1430 (2020).
[30]F. P. Mechel, *Formulas of Acoustics* (Acoustical Society of America, New York, 2004).
[31]J. Merhaut, *Theory of Electroacoustics* (McGraw-Hill College, New York, 1981).
[32]S. D. Senturia, *Microsystem Design* (Springer Science & Business Media, Dordrecht, Netherlands, 2007).
[33]W. Kampinga, Y. H. Wijnant, and A. de Boer, "Performance of several viscothermal acoustic finite elements," Acta Acust. united Acust. **96**(1), 115–124 (2010).
[34]COMSOL Multiphysics v.6.1, Acoustics Module User's Guide (2022).
[35]G. Bertotti and I. D. Mayergoyz, *The Science of Hysteresis: 3-Volume Set* (Elsevier, Oxford, UK 2005), Vol. 3.
[36]"GRAS RA0402 prepolarized high-frequency ear simulator" available at https://www.grasacoustics.com/products/ear-simulator/product/786-ra0402 (Last viewed December 21, 2023).
[37]M. R. Stinson, "Implications of ear canal geometry for various acoustical measurements," J. Acoust. Soc. Am. **74**(S1), S8 (1983).